microbial biotechnology

Open Access

Membrane composition and organization of *Bacillus subtilis* 168 and its genome-reduced derivative mini*Bacillus* PG10

Amanda Y. van Tilburg,[1,†] Philipp Warmer,[2,3,†] Auke J. van Heel,[1] Uwe Sauer[2] and Oscar P. Kuipers[1,*]

[1]*Department of Molecular Genetics, University of Groningen, Groningen, The Netherlands.*
[2]*Institute of Molecular Systems Biology, ETH Zürich, Zürich, Switzerland.*
[3]*Life Science Zürich PhD Program on Systems Biology, Zürich, Switzerland.*

Summary

A form of lateral membrane compartmentalization in bacteria is represented by functional membrane microdomains (FMMs). FMMs are important for various cellular processes and offer application possibilities in microbial biotechnology. We designed a lipidomics method to directly measure relative abundances of lipids in detergent-resistant and detergent-sensitive membrane fractions of the model bacterium *Bacillus subtilis* 168 and the biotechnologically attractive mini*Bacillus* PG10 strain. Our study supports previous work suggesting that cardiolipin and prenol lipids are enriched in FMMs of *B. subtilis*. Additionally, structural analysis of acyl chains of major phospholipids indicated that FMMs display increased order and thickness compared with the surrounding bilayer. Despite the 36% genome reduction, membrane and FMM integrity are largely preserved in mini*Bacillus* PG10, as supported by analysis of membrane fluidity, flotillin distribution and gene expression data. The novel insights in FMM architecture reported here will contribute to further explore the biological significance of FMMs and the means by which FMMs can be exploited as heterologous production platforms. Moreover, our lipidomics method enables comparative FMM lipid profiling between different bacteria.

Received 21 June, 2021; revised 13 October, 2021; accepted 14 November, 2021.
*For correspondence. E-mail o.p.kuipers@rug.nl; Tel. +31 503632093; Fax +31 50 6362348.
†These authors contributed equally.
Microbial Biotechnology (2022) **15**(5), 1633–1651
doi:10.1111/1751-7915.13978
Funding information
This work was supported by a grant from the European Union's Horizon 2020 research and innovation program (Grant Agreement No. 720776).

Introduction

In addition to serving as a physical barrier, the cytoplasmic membrane is important for a wide variety of cellular processes. Therefore, maintenance of membrane integrity, i.e. the composition and organization of membrane lipids and proteins, is critical for cell viability and function. It has become widely accepted that both eukaryotic and prokaryotic plasma membranes exhibit lateral heterogeneity in the distribution of lipids and proteins (Carquin *et al*., 2016). A well-studied example of membrane subcompartimentalization is the existence of lipid raft domains in eukaryotic plasma membranes (Simons and Ikonen, 1997). Lipid rafts are mobile sphingolipid- and cholesterol-enriched microdomains that are relatively more ordered and compact compared with the surrounding membrane. Various proteins have been found to depend on the specific lipid environment created by lipid rafts or on the marker protein of lipid rafts, flotillin (Sezgin *et al*., 2017). Furthermore, lipid rafts appear to serve as scaffolding platforms, which can promote interactions between particular proteins. Accordingly, lipid rafts have been shown to play a role in various eukaryotic processes, ranging from insulin signalling to regulation of the cytoskeleton (Otto and Nichols, 2011).

Interestingly, bacterial equivalents of eukaryotic lipid raft domains have been discovered more recently (López and Kolter, 2010). In bacteria, these liquid-ordered membrane microdomains have been defined as functional membrane microdomains (FMMs). Like eukaryotic rafts, the flotillin protein serves as marker protein of FMMs (Bramkamp and Lopez, 2015). Bacterial flotillins have been shown to influence the activity of other proteins via their scaffolding activity (Lopez and Koch, 2017) as well as by their impact on overall membrane organization (Bach and Bramkamp, 2013; Zielińska *et al*., 2020). Hence, FMMs have been implicated in a wide range of bacterial processes, among which motility, cell division, protein secretion, biofilm formation, sporulation and cell wall organization (Lopez and Koch, 2017). Notably, a recent study demonstrated that bacterial FMMs can also be exploited as spatial scaffolds in order to optimize the

production of industrial relevant compounds (Lv *et al*., 2020).

To date, most work concerning the biological significance of FMMs has been performed using *Bacillus subtilis* as a model organism. Although the two flotillins of *B. subtilis*, FloA and FloT, and their interaction partners have been quite well studied (Bach and Bramkamp, 2013; Schneider *et al*., 2015), the constituent lipids of FMMs have been left relatively unexplored. Since most bacteria do not synthesize cholesterol and sphingolipids, other types of bacterial lipids have been suggested to make up FMMs (Bramkamp and Lopez, 2015; Lopez and Koch, 2017). Firstly, linear and circular prenol lipids (composed of C_5 isoprenoid units) have been described as potential FMM constituents due to their more hydrophobic character compared with phospholipids. More specifically, the C_{15} isoprenoid lipid farnesol, and possibly derivatives thereof, seem to be important for securing FMM integrity in *B. subtilis* (López and Kolter, 2010; Bach and Bramkamp, 2013). Deletion of the farnesol biosynthetic gene (*yisP*) impaired the FMM-associated signalling pathway for biofilm formation (López and Kolter, 2010) and led to a less heterogeneous and overall more rigid membrane (Bach and Bramkamp, 2013). In addition to farnesol, carotenoids (linear C_{40} isoprenoid lipids) could be important structural and functional components of FMMs in bacteria that are capable of carotenoid production. In *Staphylococcus aureus*, the carotenoid staphyloxanthin was identified as a structural component of FMMs and as a specific lipid interaction partner of FloA (García-Fernández *et al*., 2017). Moreover, cyclic prenol lipids named hopanoids – also known as sporulenes in *B. subtilis* – might be part of FMMs as certain hopanoid species have been shown to induce the formation of liquid-ordered domains in model membranes and *in vivo* (Saenz *et al*., 2012; Doughty *et al*., 2014; Sáenz *et al*., 2015). In addition to prenol lipids, cardiolipin (CL) has been proposed as a lipid component of FMMs (Bramkamp and Lopez, 2015). CL is a negatively charged phospholipid that is formed after the dimerization of two phosphatidylglycerol molecules, with the release of one moiety of glycerol. In *B. subtilis*, CL-rich domains have been detected at the cell poles and division septa (Kawai *et al*., 2004). Furthermore, by using thin-layer chromatography, CL was found in a membrane fraction also containing flotillins (Donovan and Bramkamp, 2009). Nevertheless, FloT did not exclusively colocalize with CL domains. Therefore, a potential structural, and possibly functional, role of CL in FMMs remains to be clarified.

To increase our understanding of the biophysical basis of FMMs and their constituent lipids, we performed a detailed lipidomic analysis of FMMs in two academically and industrially relevant *B. subtilis* host strains: *B. subtilis* 168 and mini*Bacillus* PG10 (Reuß *et al*., 2017; Michalik *et al*., 2021). *B. subtilis* 168 is a commonly used laboratory strain, whereas mini*Bacillus* PG10 is a genome-minimized (by 36%) derivative of *B. subtilis* 168. Although PG10 displays a defect in the final stage of cell division (van Tilburg *et al*., 2021), it is an attractive host strain for the production of heterologous proteins and peptides (Aguilar Suárez *et al*., 2019; van Tilburg *et al*., 2020). For this purpose, we established a detergent-compatible LC-MS method in order to be able to analyse different membrane fractions isolated by detergent treatment. Whereas CL, polyprenol lipids and isoprenoids were identified as major constituent lipids of FMMs in both *B. subtilis* 168 and PG10, CL and isoprenoid lipids were even more enriched in FMMs in PG10. Moreover, similarities in flotillin distribution and membrane fluidity were observed between PG10 and its parental strain, indicating that the genome reduction did not significantly impact membrane order and structural integrity of FMMs in PG10. In line with this, only minor differences in the expression level of the majority of FMM lipid biosynthesis genes were observed between PG10 and *B. subtilis* 168. Furthermore, reintroduction of *yisP* in PG10 resulted in an overall more fluid membrane, whereas deletion of the major CL synthase (*clsA*) in PG10 reduced both the level of CL and isoprenoid lipids in FMMs. Altogether, this work sheds more light on the constituent lipids of FMMs in the bacterial model organism *B. subtilis* 168 and gives a first insight into the occurrence and integrity of FMMs in the biotechnologically attractive mini*Bacillus* PG10 strain.

Results

*Mini*Bacillus *PG10 and* B. subtilis *168 display similarities in flotillin distribution and in membrane fluidity*

Prior to lipidomic analysis, the existence of FMMs in PG10 was probed by examination of the localization of flotillins in PG10. In *B. subtilis*, the two flotillins, FloA and FloT, previously have been shown to display a punctuate pattern throughout the cytoplasmic membrane (Donovan and Bramkamp, 2009; López and Kolter, 2010). In addition, flotillins are detected in the detergent-resistant membrane (DRM) fraction, which is considered to be enriched in FMMs (Brown, 2002). In contrast, the detergent-sensitive membrane (DSM) fraction reflects the more fluid and disordered parts of the membrane. To examine the localization of FloA and FloT in PG10, each of the flotillins was translationally fused to GFP and the localization of the fusion proteins was analysed when expressed from their natural promoters. Fluorescence microscopy showed a heterogeneous distribution of each of the flotillins throughout the membrane and indicated the existence of FloA and FloT foci in both *B. subtilis* 168 and PG10 (Fig. 1A and B). Furthermore, Western blot analysis revealed the enrichment of FloA and FloT in

the DRM fraction of PG10, similar as observed for *B. subtilis* 168 (Fig. 1C and D). These results thus suggest that PG10 still forms flotillin-containing FMMs in its membrane.

Since membrane fluidity is crucial for cellular integrity and may be affected by the genetic deletions, we determined fluidity with Laurdan staining. This was of particular interest, since PG10 lacks YisP, a phosphatase that produces farnesol and which is important for maintenance of membrane heterogeneity in *B. subtilis* 168 (López and Kolter, 2010; Feng *et al*., 2014). Laurdan spectroscopic measurements resulted in similar generalized polarization (GP) values for *B. subtilis* 168 and PG10, in both the exponential and stationary growth phase (Fig. 2A). In addition, by using Laurdan fluorescence microscopy regions of high and low fluidity could be observed in the membrane of *B. subtilis* 168 and PG10 (Fig. 2B). Thus, both the overall and local membrane organization seem comparable between PG10 *B. subtilis* 168 in terms of lipid ordering.

Setup of the lipidomics method and comparison of total membrane lipid composition

To profile the lipid composition of the membrane and FMMs of *B. subtilis* 168 and mini*Bacillus* PG10, three membrane fractions were prepared in triplicate for each strain: total membrane (TM), DRM fraction (parts of the membrane containing FMMs) and DSM fraction (non-FMM membrane). It is essential to use a mixture of non-ionic detergents to separate the membrane fraction containing FMMs from the rest of the membrane, since lipid rafts can resist disaggregation by the detergents (Brown, 2002). Therefore, we designed a detergent-compatible LC-MS/MS method that entails a valve switch in conjunction with a chromatographic gradient to separate the detergents from the analytes (Fig. 3A). In each chromatographic run, the initial flow-through was discarded and the eluting clean lipid matrix was injected into the mass spectrometer. Data were acquired in positive/negative ionization switching mode using Top20 MS2 acquisition, resulting in broad lipidomic coverage with a runtime of 30 min per sample. A total of 8959 compound groups mapping to 576 lipids were detected across all samples. Annotation of detected ions to actual lipids was done using an in-house lipid mass list based on lipid maps (Fahy *et al*., 2005, 2009). We performed total ion current (TIC) normalization, resulting in the relative quantification of the different lipid classes in the different samples of *B. subtilis* 168 and PG10. While this relative quantification approach enables the comparison between samples, it is limited to intra-class comparison and does not allow for inter-class comparisons. Hierarchical clustering of z-scored relative lipid abundances indicated that the DRM fractions cluster separately from the DSM and TM fractions (Fig. 3B). In addition, within the DRM cluster, the samples of *B. subtilis* 168 and PG10 formed two distinct groups, suggesting differences in FMM lipid profiles between the two strains.

First, we focussed on the total membrane fraction to ask whether the genome reduction altered the lipid composition. Phosphatidylglycerol (PG) and phosphatidylethanolamine (PE) previously have been reported as major components of the phospholipid profile of *B. subtilis*, whereas CL is relatively less abundant (Gidden *et al*., 2009; Bernat *et al*., 2016). Determination of TIC normalized relative abundances per lipid class revealed the same trend in relative abundance of these phospholipids in TM fractions of our strains (Fig. 3C). In both strains, PG was found to be the most abundant phospholipid, followed by PE and CL. In addition, no differences were observed in the most abundant lipid species in the membrane of *B. subtilis* 168 and PG10 (Fig. 3D), indicating that the bulk of the membrane is similar between the strains. Also for the other lipid classes, no significant changes in relative abundance were observed between the two strains (Fig. S1). The only visibly affected lipid classes were polyprenols, free fatty acids and hopanoids, of which the two latter classes seemed to be decreased in the membrane of PG10. Despite the genome reduction of ~ 36%, the above data thus show that the membrane of PG10 and *B. subtilis* 168 is largely similar in lipid composition.

CL is the main lipid component of FMMs in B. subtilis *168*

Bacterial lipid rafts have been suggested to be enriched in prenol lipids (e.g. isoprenoids) and CL (Donovan and Bramkamp, 2009; López and Kolter, 2010; Bach and Bramkamp, 2013; García-Fernández *et al*., 2017). However, these assumptions are based on limited experimental evidence. Here, we measured for the first time whether an enrichment of these lipid classes could be retrieved in the FMM-containing membrane fraction (DRM) of *B. subtilis* 168 by using the designed lipidomics method. Comparison of TIC normalized relative abundances per lipid class between the DRM and DSM fraction of *B. subtilis* 168 revealed CL to be most strongly enriched in the DRM fraction (Fig. 4A). In addition, we found that polyprenols and isoprenoids of the raft-associated lipid category of prenols were among the most differential lipids, together with PE and DAG lipids (Fig. 4B). A detailed breakdown of detected prenol lipids can be found in Fig. S2. Zooming in on the difference in class abundance with single lipid species resolution, we found that only CL and polyprenols had significantly (q-value <= 0.01) unidirectionally increased lipid species in the DRM fraction (Fig. 4C). PE and DAG showed significant bidirectional changes. The largest alteration

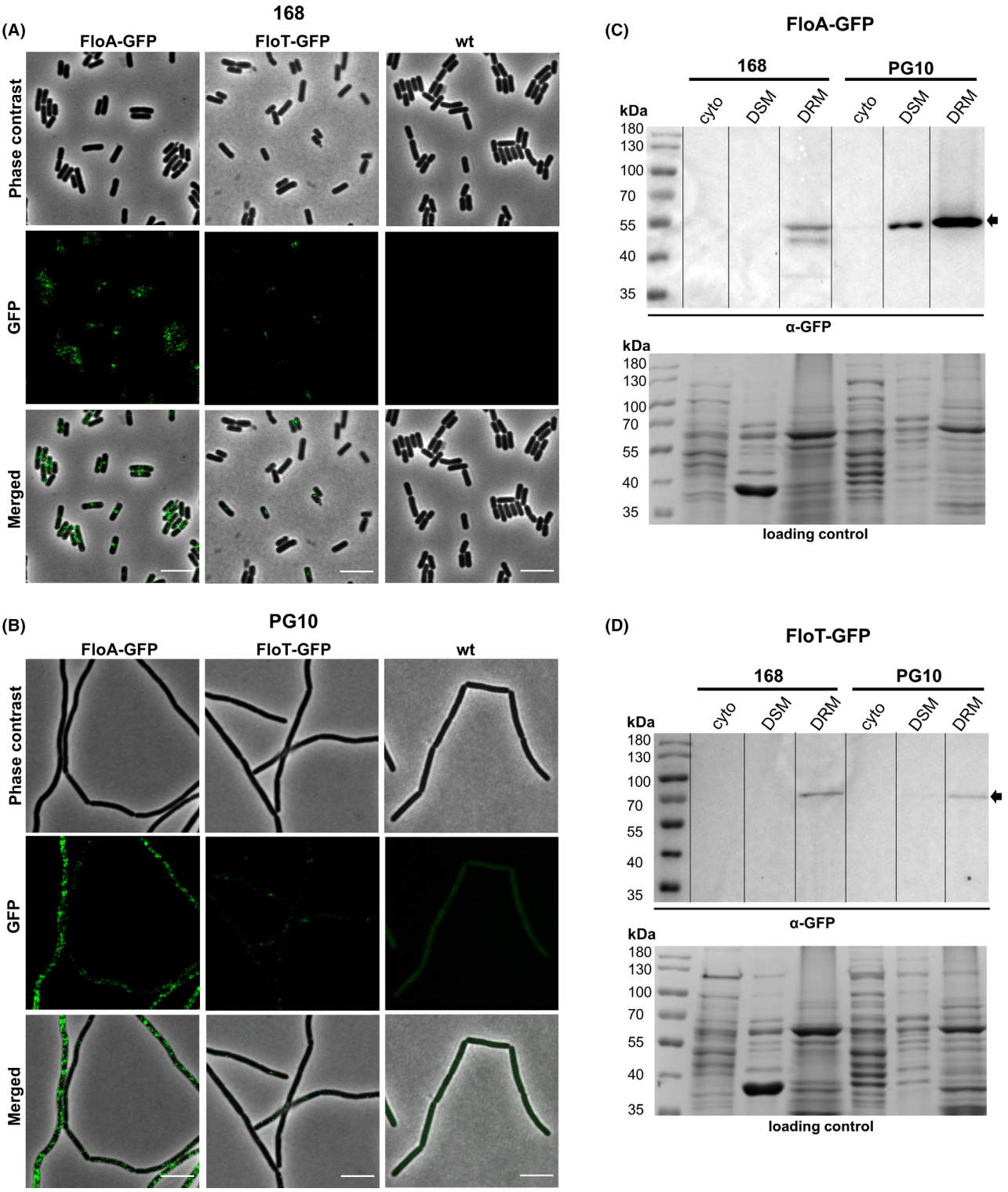

Fig. 1. Localization of flotillins in mini*Bacillus* PG10 and *B. subtilis* 168. Localization of FloA and FloT was assessed by fusion to GFP (green fluorescent protein) and when expressed from their natural promoters by fluorescence microscopy (A and B), and Western blotting (C and D). In (A) and (B), phase contrast, GFP and merged images of these two channels are shown for each strain. Pictures were taken of cells in late-exponential to stationary phase, grown in LB-Miller medium. Scale bars are 5 μm. In (C) and (D), three cellular fractions of each strain were analysed: cyto = cytosol, DSM = detergent-sensitive membrane fraction, DRM = detergent-resistant membrane fraction (FMM-enriched fraction). Arrows indicate the height at which FloA-GFP (63 kDa) and FloT-GFP (84 kDa) were detected. Coomassie-stained SDS-PAGE gels are shown as loading controls.

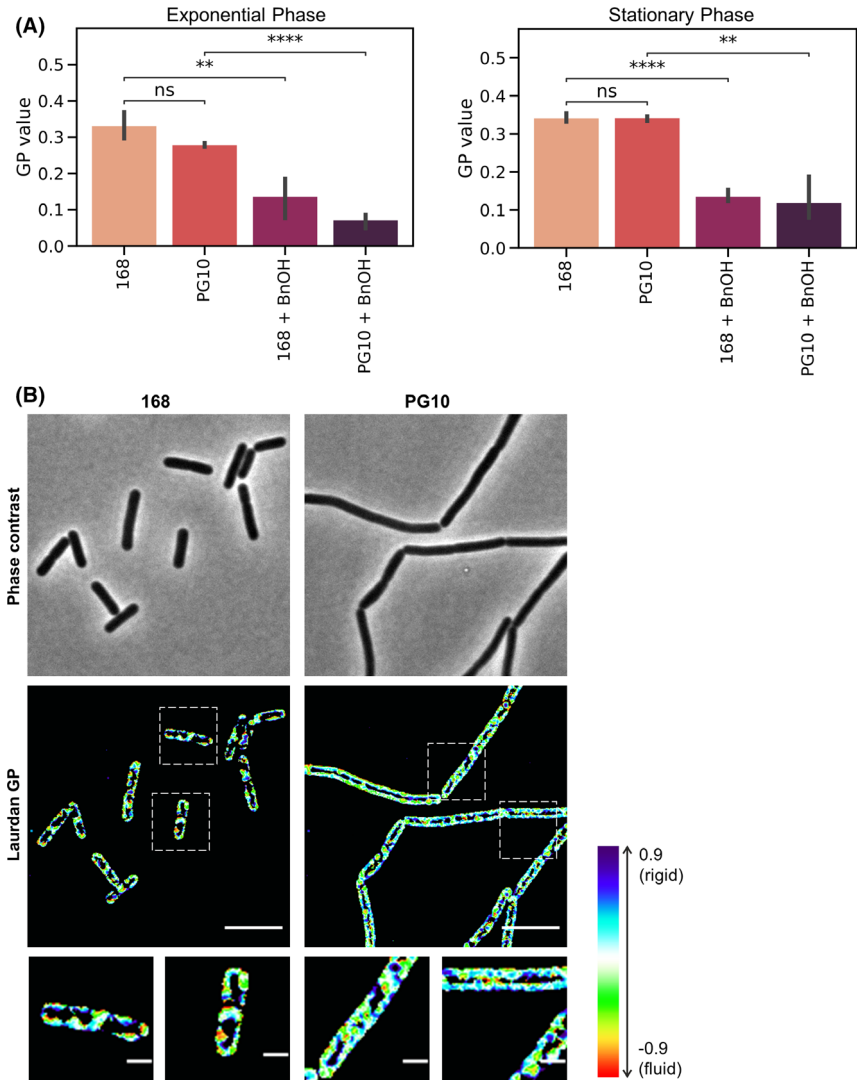

Fig. 2. Mini*Bacillus* PG10 and *B. subtilis* 168 display similarities in membrane fluidity.
A. Laurdan GP values calculated from spectroscopic measurements of cell cultures labelled with Laurdan. GP values were determined in the exponential and stationary growth phase for *B. subtilis* 168 and PG10. Benzyl alcohol (BnOH) was used as a control that acts as membrane fluidizer. Confidence interval (95%) shown as error bar, significant levels calculated using Student's unpaired *t*-test ($n = 3$), *P*-value $\leq$ 0.05, 0.01, 0.001, 0.0001 represented as *, **, ***, ****. Not significant abbreviated with ns.
B. Laurdan microscopic analysis of *B. subtilis* 168 and PG10 at exponential phase. Laurdan GP values were calculated using ImageJ and a range from −0.9 (fluid) to 0.9 (rigid) was used. Phase contrast, Laurdan GP and zoomed images of Laurdan GP (white boxes) are shown. Scale bars are 5 μm (main images) and 1 μm (zoomed images).

between the DRM and DSM fraction with the most significant fold change was CL (64:0).

We conclude that using the detergent-compatible lipidomics method, we can measure and cluster especially the DRM fractions in distinct groups based on their lipidomic profile. Furthermore, we found that, as expected, both CL as well as prenols are enriched in the DRM fraction. Among those lipid classes, the most abundant species were CL (64:0), the CL species made from PG (32:0), and an isomeric compound corresponding to polyprenol (35:9) a bactoprenoldiphosphate (Fig. S3). Strikingly, hopanoids were more abundant in the DSM fraction of *B. subtilis*. Equipped with this lipidomics method, capable of untargeted profiling of FMM lipids in complex detergent-containing matrix, we next could analyse the DRM fraction of mini*Bacillus* PG10.

*Enrichment of hopanoids, CL and isoprenoids in the DRM of mini*Bacillus *PG10 compared with* B. subtilis *168, whereas structural properties of phospholipids remain unchanged*

We speculated that the lipid composition of FMMs in mini*Bacillus* PG10 might be different compared with its

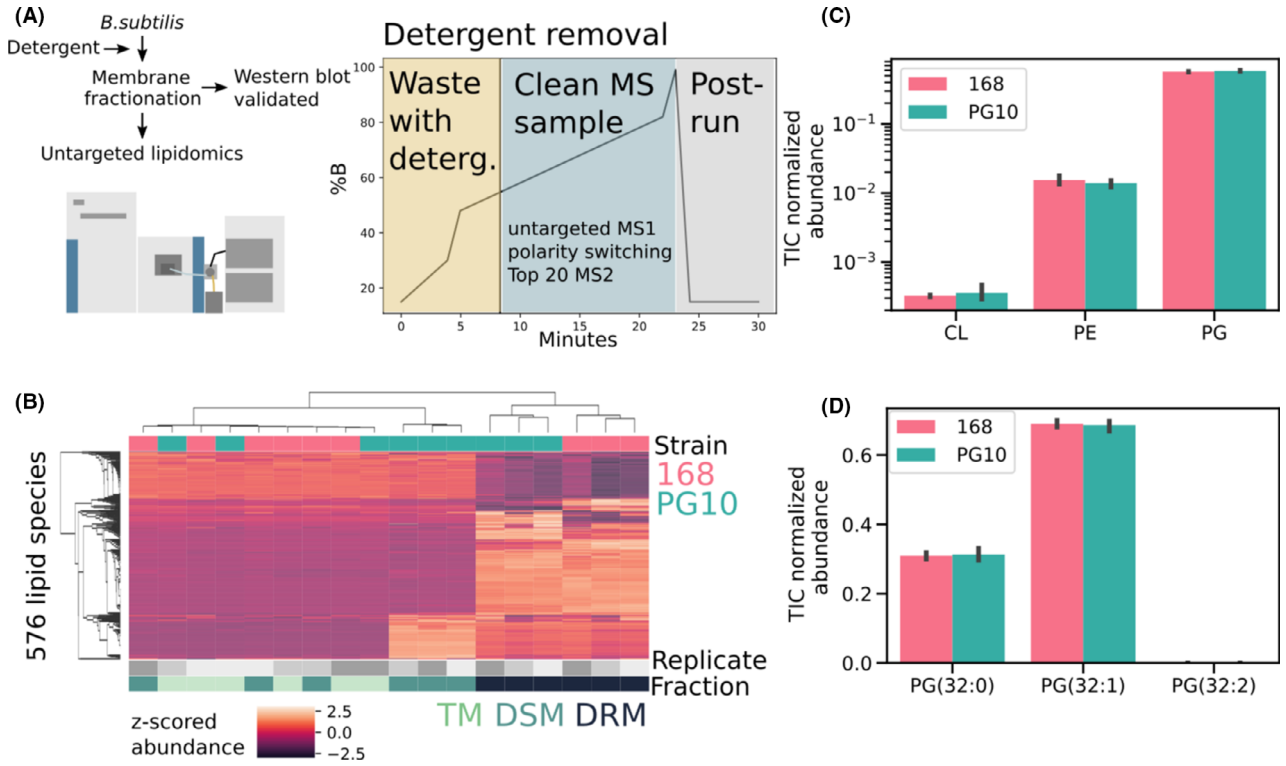

Fig. 3. Setup for lipidomic analysis of FMMs and comparison of total membrane composition.
A. Profiling method using a valve switch to discard the detergents for untargeted raft lipidomics.
B. Heatmap of all z-scored relative lipid abundances in *B. subtilis* 168 and PG10 across total membrane (TM), detergent-sensitive membrane fraction (DSM) and detergent-resistant membrane fraction (DRM).
C. TIC normalized relative abundance comparison of the main lipid classes in the TM fractions of *B. subtilis* 168 and PG10.
D. Most abundant PG lipid species with different number of double bonds in the TM fractions of *B. subtilis* 168 and PG10. Abbreviations: cardiolipin (CL), phosphatidylglycerol (PG), phosphatidylethanolamine (PE) and detergent (deterg.).

parental strain, due to absence of the farnesol-producing enzyme YisP, which in *B. subtilis* 168 has been shown to be important for the functionality of FMM-associated processes (López and Kolter, 2010). Therefore, we compared the DRM fractions between PG10 and *B. subtilis* 168. In addition to differences in lipid class abundance and specific lipid alterations, we compared the structural properties of the main phospholipids across the different membrane fractions.

We found that the overall lipid class composition, while being mostly similar (Fig. 5A), also had distinct features (Fig. 5B). In particular, hopanoids, CL as well as isoprenoids were enriched in the DRM fraction of PG10, whereas mainly PE and DAG were more abundant in the DRM fraction of *B. subtilis* 168. The study of the individual lipid species revealed that CL and the prenol lipid class isoprenoids only had significantly increased species in PG10, while the only uniquely decreased lipid was FA (16:1), a generic lipid precursor (Fig. 5C). Next, we investigated the degree of saturation and the length of acyl chains in the phospholipids between the different membrane fractions and in particular between the two *B. subtilis* strains. We expected that especially the FMM-containing membrane fraction would have longer fatty acids with a high degree of saturation, thereby giving the region its compact and low fluidity characteristics (Bramkamp and Lopez, 2015). To this end, we computed the relative abundance-weighted average number of double bonds and acyl chain length per acyl chain for the main phospholipids of *B. subtilis*, PE, PG and CL (Fig. 5D and E). In agreement with our expectation, we found that acyl chains of phospholipids in the DRM fraction are longer and have less double bonds compared with phospholipids of the TM and DSM fractions, corresponding to less fluid and more compact parts of the membrane. This difference was driven by each of the three main phospholipids, except for PE regarding acyl chain length. While in DRM fractions the lipid classes had a similar acyl chain composition, their structure is more variable in the DSM fractions. Furthermore, we compared odd and even chained phospholipids and compared their degree of saturation of relevant acyl chains as a proxy for branched chain fatty acids. However, no striking differences were observed (Fig. S4).

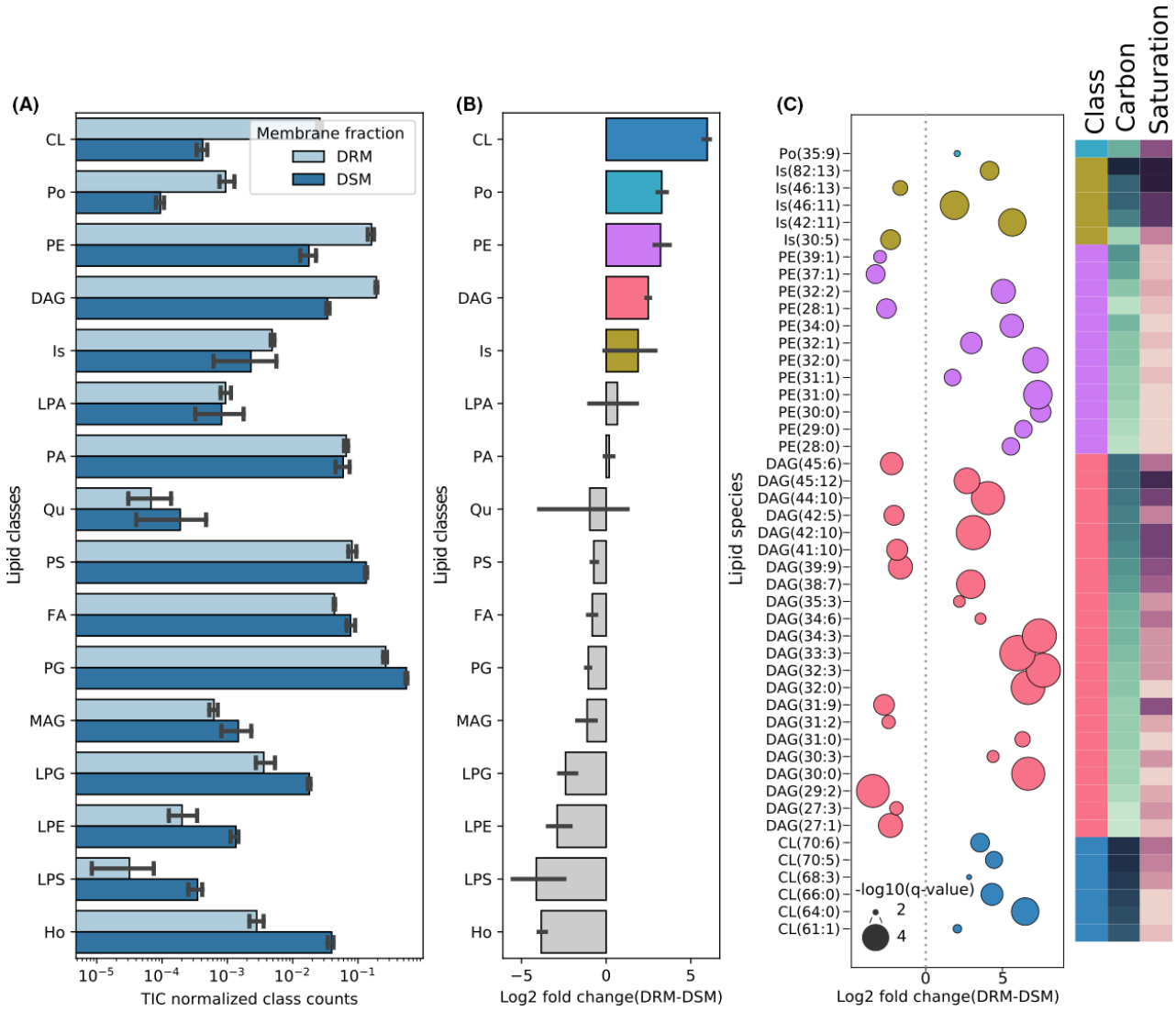

Fig. 4. Comparison of DRM and DSM membrane fraction in *B. subtilis* 168.
A. TIC normalized relative abundance comparison of all detected lipid classes in DRM and DSM fractions of *B. subtilis* 168.
B. Log2 fold change between DRM and DSM of *B. subtilis* 168 sorted by median fold change; the five lipid classes increased in DRM are coloured.
C. Significantly changing lipids (*q*-value <= 0.01) of the five most increased lipid classes between DRM and DSM of *B. subtilis* 168. Benjamini–Hochberg corrected *q*-values from Student's unpaired *t*-test. Dot size reflects -log10 transformed *q*-value. Abbreviations: cardiolipin (CL), polyprenol (Po), phosphatidylethanolamine (PE), diacylglycerol (DAG), isoprenoids (Is), lysophosphatidic acid (LPA), fatty acid (FA), phosphatidylglycerol (PG), quinones (Qu), phosphatidylserine (PS), monoacylglycerol (MAG), lysophosphatidylglycerol (LPG), lysophosphatidylethanolamine (LPE), lysophosphatidylserine (LPS) and hopanoids (Ho).

Our data thus show that the relative abundance of lipid classes in the DRM fraction of PG10 differs from the DRM of *B. subtilis* 168, highlighted by increased levels of CL and prenol lipids. This suggests FMMs to be even more ordered in PG10. However, the structural properties of DRM phospholipids, such as degree of saturation and length of acyl chains, are similar between the two strains, but noticeably different from the non-raft membrane. The structural lipidome divergence in the stationary phase, which has been described elsewhere (Chwastek *et al.*, 2020), was only absent in the DRM fraction. This indicates that distinct sets of biochemical processes work on the different membrane fractions.

Putative association between the abundance of CL and isoprenoids

While the saturation level and acyl chain length of phospholipids in the DRM fraction were comparable between *B. subtilis* 168 and mini*Bacillus* PG10, the class

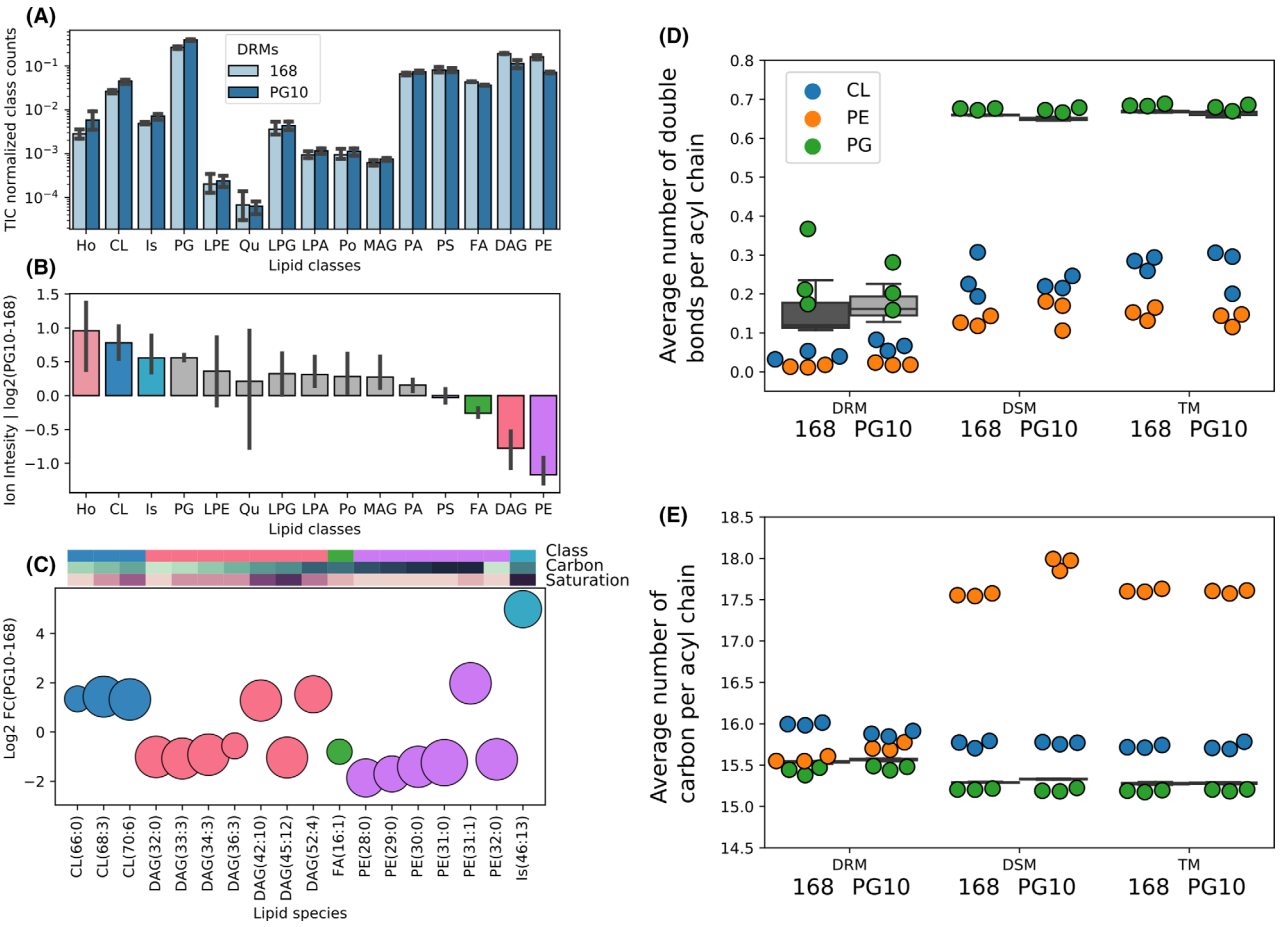

Fig. 5. Comparison of DRM lipid composition and structural properties of main phospholipids between PG10 and 168.
A. Relative abundance comparison of all detected lipid classes in the DRM of PG10 and 168.
B. Log2 fold change of lipid classes in the DRM fraction of PG10 compared with 168.
C. Significantly changing lipids (q-value <= 0.01) of the top 3 most differential lipid classes in the DRM of PG10 and 168. Benjamini–Hochberg corrected q-values from Student's unpaired t-test. Dot size reflects −log10 transformed q-value.
D. Weighted average number of double bonds per acyl chain of the most abundant membrane phospholipids, PG, PE and CL, on the class level as coloured dots, and as bulk, grey boxplot.
E. Weighted average number of acyl chain length per acyl chain of the most abundant membrane phospholipids, PG, PE and CL, on the class level as coloured dots, and as bulk, grey boxplot. Abbreviations: cardiolipin (CL), polyprenol (Po), phosphatidylethanolamine (PE), diacylglycerol (DAG), isoprenoids (Is), lysophosphatidic acid (LPA), fatty acid (FA), phosphatidylglycerol (PG), quinones (Qu), phosphatidylserine (PS), monoacylglycerol (MAG), lysophosphatidylglycerol (LPG), lysophosphatidylethanolamine (LPE), lysophosphatidylserine (LPS) and hopanoids (Ho).

composition was altered, especially in CL and prenol lipids. To study the relationship between these lipid groups, we tested several PG10 mutant strains in which possibly one of these lipid groups would be modulated. Since CL was confirmed to be a major constituent lipid of FMMs, membrane properties and lipidome composition of a PG10 strain lacking the major CL synthase (*clsA*) were assessed. In addition, since PG10 lacks *yisP*, encoding a phosphatase implicated in membrane organization in *B. subtilis* (Bach and Bramkamp, 2013), two PG10 strains in which *yisP* was reinserted in the genome were analysed (controlled by either its natural promoter P_{nat} or by the strong constitutive P_{veg} promoter, which is 50 times stronger than P_{nat}).

By using Laurdan staining, we first assessed whether deletion of *clsA* or reintroduction of *yisP* affected overall membrane fluidity in PG10. For each of the three mutant strains, a decreased GP value was observed compared with PG10 wild type (Fig. 6A). These results indicate that both depletion of CL as well as reintroduction of *yisP* results in a more fluid membrane. Lipidomics analysis showed that CL levels were decreased by two orders of magnitude in the DRM fraction of the *clsA* knockout mutant (Fig. 6B). Interestingly, this expected change coincided with a decrease in isoprenoid levels (Fig. 6B and Fig. S3). For the PG10 strains with reintroduced *yisP*, no difference in any of the lipid classes was observed (Fig. 6B and Fig. S5). Next, we analysed the

acyl chain structure, which is known to most strongly affect fluidity, i.e. the number of double bonds. Since Laurdan staining indicated a slightly more fluid membrane for the *yisP* strains, we hypothesized that especially for those strains the saturation state of phospholipids might be decreased, thereby contributing to a more fluid membrane. Corroborating our hypothesis, we found that both PG10 strains with *yisP* reintroduced displayed an increase in fatty acid double bonds in the DSM fraction, but not in the DRM fraction (Fig. 6C). In contrast, PG10 Δ*clsA* showed no significant differences in the phospholipidome saturation state neither in the DSM nor DRM fraction (Fig. 6C).

Based on the coinciding decrease in CL and isoprenoids in the *clsA* knockout, we hypothesize that a putative association between the two lipid classes exists. While the reintroduction of *yisP* resulted in an increase in the number of double bonds, thereby affecting fluidity, no effect on the FMM lipid composition was observed.

RNA-seq analysis largely correlates with lipidomic profiles of B. subtilis *168 and PG10*

To investigate whether we could find an underlying genetic basis for the observed lipidome profiles of *B. subtilis* 168 and PG10, RNA-seq analysis was performed. In addition to explaining differences in membrane and/or DRM composition between the two strains, transcriptomic analysis might serve as an additional quality control for the similarities that were observed between the two strains. Although changes at the transcriptome level previously have been described for PG10 versus its progenitor strain Δ6 (Reuß *et al*., 2017), we here performed RNA-seq analysis for PG10 and *B. subtilis* 168 to allow a good comparison to our lipidomics data. For this purpose, RNA was isolated from *B. subtilis* 168 and PG10 cultures in the late-exponential growth phase and in the stationary growth phase. Even though lipidomic samples had been prepared from cells grown till stationary phase, we reasoned that gene expression

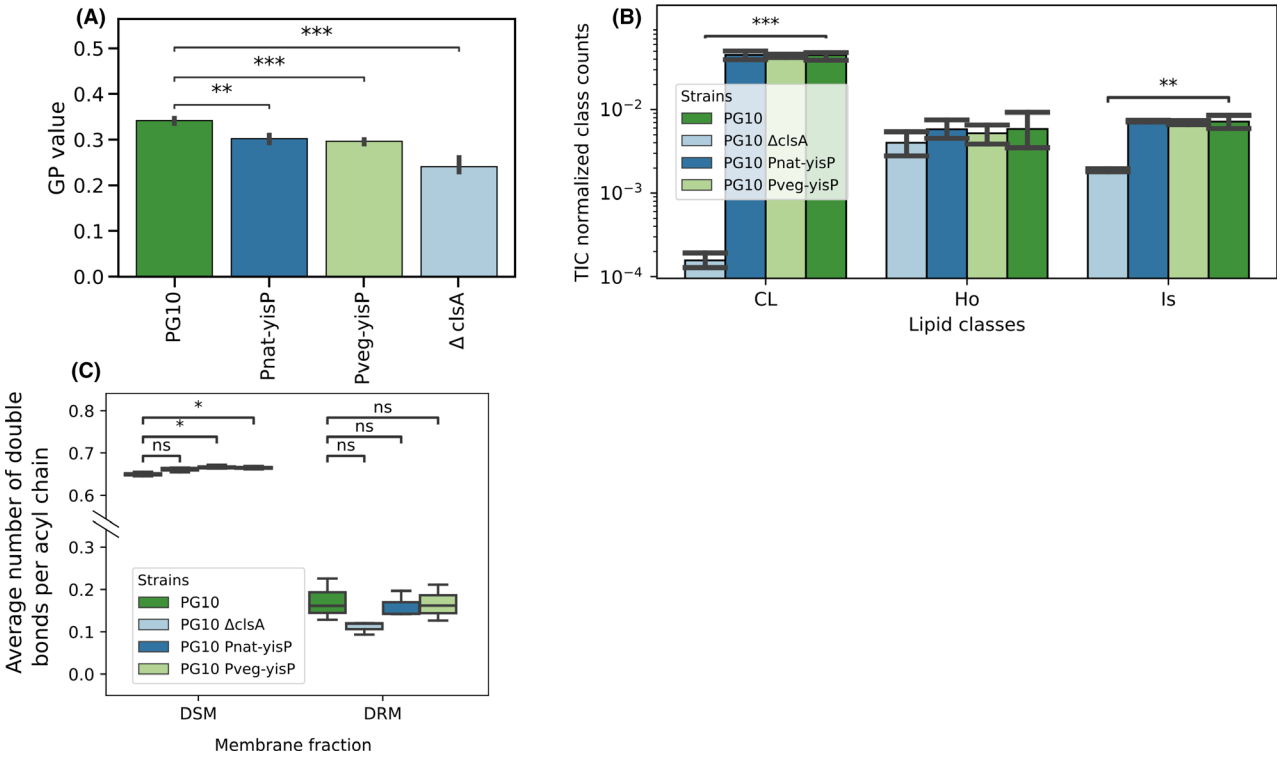

Fig. 6. Effect of deletion of *clsA* or reintroduction of *yisP* on PG10 membrane fractions.
A. Laurdan GP values calculated from spectroscopic measurements of cell cultures labelled with Laurdan. GP values were determined in the stationary growth phase.
B. Relative abundance of FMM lipids in the DRM fraction of PG10 Δ*clsA* and in PG10 strains with reintroduced *yisP* (controlled by the native *yisP* promoter (P_{nat}) or a strong constitutive promoter (P_{veg})). P_{veg} is 50 times stronger than P_{nat}. Abbreviations: cardiolipin (CL), hopanoids (Ho) and isoprenoids (Is).
C. Weighted average number of double bonds per acyl chain of the major phospholipids PE, PG and CL in DSM and DRM fractions of PG10 wt, PG10 Δ*clsA* and PG10 strains containing *yisP*. Error bar as 95% confidence interval, significant levels calculated using Student's unpaired *t*-test ($n = 3$), *P*-value ≤ 0.05, 0.01, 0.001 represented as *, **, ***. Not significant is abbreviated with ns.

analysis in the exponential phase might also be of interest, since cells are then more metabolically active and FMMs are maturing.

PCA analysis and correlation analysis indicated distinct expression profiles for *B. subtilis* 168 and PG10 in both growth phases (Fig. S6). In addition, the three replicates of each condition showed high similarity. Gene Ontology enrichment analysis revealed lipid metabolism as one of the cellular processes to be moderately, but significantly (p-value < 0.05), affected at the transcriptome level between *B. subtilis* 168 and PG10, in both growth phases. To investigate which lipid metabolic pathways were mostly affected, differential gene expression levels were analysed of phospholipid biosynthetic genes as well as of FMM-related genes (involved in biosynthesis of prenol lipids and CL). Regarding phospholipid metabolic pathways, a general trend in the differential expression of genes involved in fatty acid metabolism was observed (Fig. 7). The majority of genes involved in malonyl-CoA production (the fatty acid precursor), biosynthesis or degradation of fatty acids and regulation of fatty acid metabolism were downregulated in PG10 in both growth phases. In addition, most of these genes displayed a fold change higher than our cut-off value of 1.4 (Table 1). These findings agree with our lipidomic analysis in which fatty acids were found to be relatively less present in the membrane of PG10 compared with *B. subtilis* 168 (Fig. S1). Nevertheless, the trend of downregulation of genes did not clearly continue for the more downstream phospholipid biosynthetic genes (e.g. *plsY*, *plsC*, *cdsA*, *pssA* and *psd*). In agreement with this, the relative abundance of the major phospholipids was not significantly different between the membranes of the two strains.

Analysis of FMM-related genes indicated a decreased expression level of both flotillins in PG10 in the exponential phase (about threefold), whereas *floT* was slightly upregulated in PG10 in the stationary phase (almost twofold) (Fig. 8 and Table 2). In addition, the heatmaps showed an overall lower expression level of genes involved in the biosynthesis of FMM lipids (prenol lipids and CL) in PG10, especially in the exponential phase. However, not all genes displayed this trend. For instance, some genes of the MEP pathway (production of isoprenoid precursors) were upregulated in PG10. Moreover, when looking at the differential gene expression values of isoprenoid biosynthetic genes (Table 2), only a subset of genes displayed a fold change higher than our cut-off value, and changes were only minor and bidirectional. This agrees with the similar relative amount of isoprenoids in the membrane of *B. subtilis* 168 and PG10 (Fig. S1). The increased level of isoprenoids in the DRM of PG10 compared with the DRM of *B. subtilis* 168 thus seems a consequence of a larger enrichment of isoprenoids in the DRM of PG10. Interestingly, of the prenol biosynthetic genes, the only more strongly downregulated gene in PG10 was *sqhC* (12-fold in stationary phase). Since *sqhC* encodes a squalene–hopene cyclase, its downregulation in PG10 might explain the decreased level of hopanoids in the membrane of PG10. When focussing on the polyprenol biosynthetic genes (*hepS*, *hepT* and *uppS*), only a significant decrease in expression level was found for *hepS* and *hepT* in PG10. These genes encode a heptaprenyl diphosphate synthase complex, which is responsible for the biosynthesis of polyprenol diphosphates composed of seven isoprene units. Since the class of polyprenols was increased in the membrane of PG10, these findings do not support each other. Nevertheless, we cannot rule out the possibility that yet to be identified genes involved in the biosynthesis of polyprenol lipids were excluded from our RNA-seq analysis.

Regarding CL biosynthesis, expression of the major CL synthase, *clsA*, was only slightly affected in the stationary phase, displaying a 1.6 times increase in PG10. Since ClsA activity determines the level of CL in both *B. subtilis* 168 and PG10 (Cao *et al.*, 2017 and Fig. 6B), the slight upregulation of *clsA* in PG10 might explain the increased enrichment of CL in the DRM fraction of PG10 compared with *B. subtilis* 168.

In toto, our RNA-seq analysis thus identifies downregulation of fatty acid metabolic genes as the most prominent change in gene expression among lipid biosynthetic genes between *B. subtilis* 168 and PG10. This finding agrees with our lipidomic analysis, in which fatty acids were the mostly affected, and decreased, lipid class in the membrane of PG10. In addition, the fact that mostly minor changes were observed in the expression level of FMM biosynthesis genes between *B. subtilis* 168 and PG10 correlates with the largely similar lipidomic profiles of the DRMs of the two strains.

Discussion

Research on bacterial lipid raft domains mainly has been focussed on the protein cargo of FMMs: the flotillin marker proteins and other proteins that depend for their functionality on FMMs. In contrast, to date, only limited data are available about the lipids that make up bacterial lipid rafts. Based on structural similarity to lipids in eukaryotic lipid rafts, model membrane studies and limited *in vivo* experiments, particular bacterial lipid classes have been suggested to be part of FMMs (Donovan and Bramkamp, 2009; López and Kolter, 2010; Sáenz *et al.*, 2015; García-Fernández *et al.*, 2017). The work presented here, for the first time, provides a direct and more detailed analysis of the lipid composition of FMMs and their structural properties in two relevant *B. subtilis* host

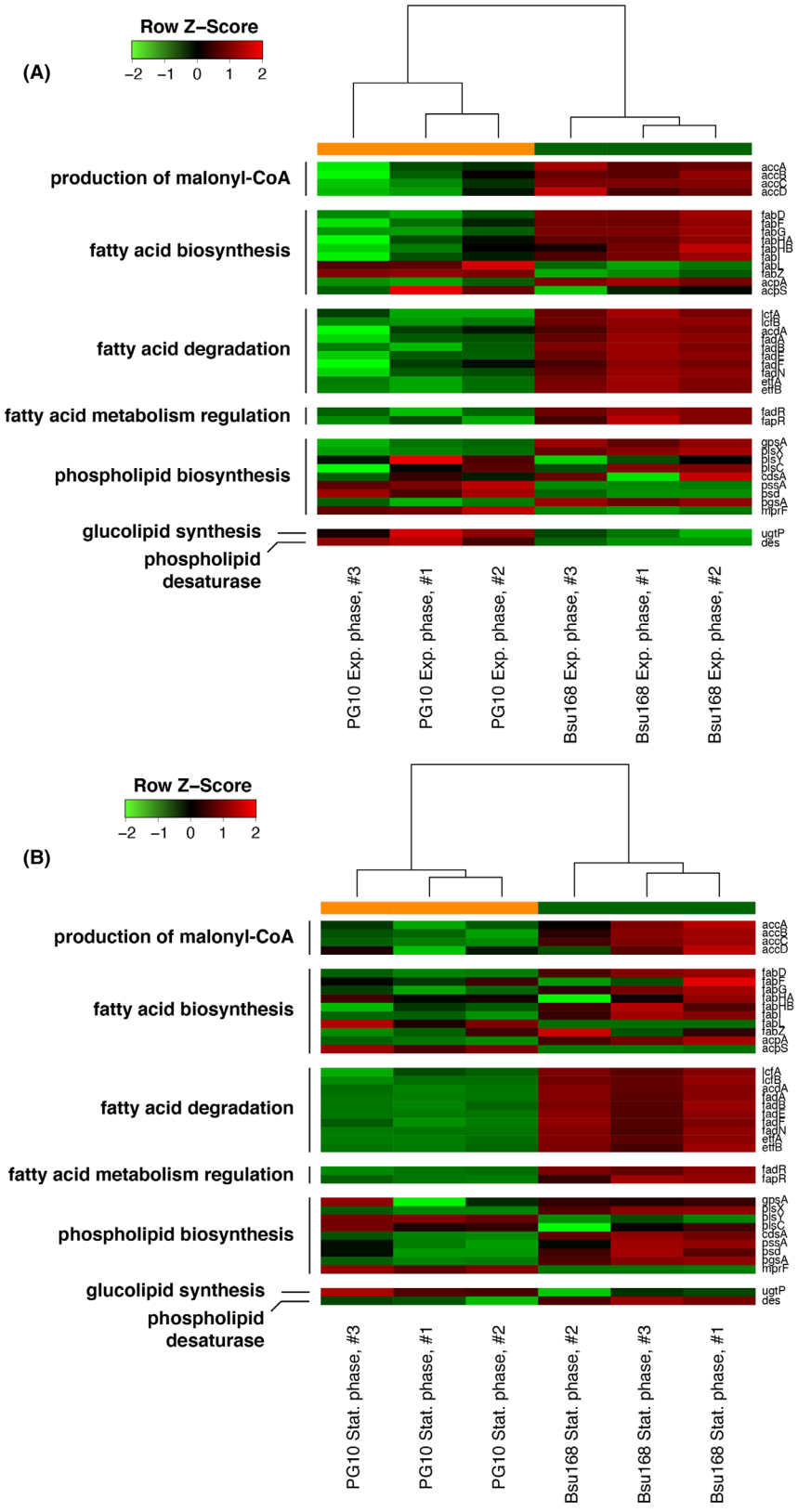

Fig. 7. Transcriptomic analysis of phospholipid metabolism in *B. subtilis* 168 and PG10. Heatmaps of gene expression profiles of phospholipid metabolic pathways (except cardiolipin biosynthetic genes) of PG10 versus *B. subtilis* 168 in exponential (A) and stationary (B) phase.

Table 1. Differential expression levels of genes involved in phospholipid biosynthesis between PG10 and *B. subtilis* 168. Only genes with fold change > 1.4 and FDR-adjusted *P*-value < 0.05 in the exponential (Exp.) and/ or stationary (Stat.) phase are shown.

Locus	Gene name	Function/pathway	Fold change PG10 vs. 168	
			Exp.	Stat.
BSU29200	*accA*	Production of malonyl-CoA		−1.5
BSU24350	*accB*	Production of malonyl-CoA		−3.7
BSU24340	*accC*	Production of malonyl-CoA	−2.9	−7.0
BSU15900	*fabD*	Fatty acid biosynthesis	−2.7	−5.6
BSU11340	*fabF*	Fatty acid biosynthesis	−3.0	
BSU15910	*fabG*	Fatty acid biosynthesis	−2.9	−2.9
BSU11330	*fabHA*	Fatty acid biosynthesis	−2.3	
BSU10170	*fabHB*	Fatty acid biosynthesis	−2.3	−3.4
BSU11720	*fabI*	Fatty acid biosynthesis	−2.1	−5.5
BSU08650	*fabL*	Fatty acid biosynthesis	1.4	2.4
BSU36370	*fabZ*	Fatty acid biosynthesis	4.1	
BSU15920	*acpA*	Fatty acid biosynthesis	−2.9	−7.5
BSU04620	*acpS*	Fatty acid biosynthesis		3.4
BSU28560	*lcfA*	Fatty acid degradation	−1.6	−1.9
BSU10270	*lcfB*	Fatty acid degradation	−4.0	−3.4
BSU37170	*acdA*	Fatty acid degradation	−2.8	−8.3
BSU32830	*fadA*	Fatty acid degradation	−7.9	−14.0
BSU28540	*fadB*	Fatty acid degradation	−2.6	−3.0
BSU32820	*fadE*	Fatty acid degradation	−8.9	−18.4
BSU37180	*fadF*	Fatty acid degradation	−2.8	−4.0
BSU32840	*fadN*	Fatty acid degradation	−6.3	−5.7
BSU28520	*etfA*	Fatty acid degradation	−3.5	−4.9
BSU28530	*etfB*	Fatty acid degradation	−3.0	−3.5
BSU28550	*fadR*	Regulator of fatty acid metabolism	−2.3	−3.5
BSU15880	*fapR*	Regulator of fatty acid metabolism		−1.6
BSU22830	*gpsA*	Phospholipid biosynthesis	−1.6	
BSU15890	*plsX*	Phospholipid biosynthesis	−2.0	−2.7
BSU18070	*plsY*	Phospholipid biosynthesis		3.1
BSU16540	*cdsA*	Phospholipid biosynthesis		−1.9
BSU02270	*pssA*	Phospholipid biosynthesis	1.8	−1.8
BSU02290	*psd*	Phospholipid biosynthesis	1.7	−1.8
BSU16920	*pgsA*	Phospholipid biosynthesis	−2.1	−2.0
BSU08425	*mprF*	Phospholipid biosynthesis	2.4	8.5
BSU19180	*des*	Phospholipid desaturase	4.1	−2.8

strains. We developed a LC-MS/MS approach in order to be able to perform lipidomic analysis on detergent-rich membrane fractions. Using the relative lipid quantities derived from this method, we confirmed that CL, isoprenoid lipids and polyprenol lipids are enriched in the FMM-containing membrane fraction (DRM) of *B. subtilis*. In particular, CL (64:0) and polyprenol (35:9) were identified as major lipid species of FMMs. Due to the large variety of possible isomers of prenol lipids, which we also observed for Po (35:9), the exact nature of polyprenols and isoprenoid lipids residing in FMMs remains a question for future research.

Surprisingly, hopanoids, a class of cyclized prenyl lipids, were found to be enriched in the DSM fraction of *B. subtilis*. This is an unexpected finding, since hopanoids have been described as structural and functional analogues of cholesterol (Saenz *et al*., 2012; Doughty *et al*., 2014; Sáenz *et al*., 2015), which is part of eukaryotic lipid rafts. However, to the best of our knowledge, the relationship between FMMs and hopanoids so far only has been studied *in vivo* in Gram-negative bacteria and cyanobacteria. Also, it has been shown that structural differences between hopanoids impact their distribution in the membrane and their ability to modulate membrane fluidity (Poger and Mark, 2013; Belin *et al*., 2018). It thus seems that the majority of hopanoid species produced by *B. subtilis* reside in the non-raft part of the membrane and this is likely due to their specific structures. Nevertheless, we also detected hopanoids in the DRM fraction. Therefore, it remains important to identify the specific structural properties of hopanoid species associated with the different membrane fractions.

In addition to the relative quantification of lipid classes enriched in FMMs, structural insights were acquired by our lipidomic analyses. Our data indicate that the acyl chains of phospholipids in FMMs are more saturated and longer compared with the phospholipids in the rest of the membrane. This agrees with the fact that lipid rafts are relatively more ordered and compact membrane regions compared with the surrounding membrane. Moreover, this suggests an increased thickness of the bilayer within bacterial lipid rafts, similar as mentioned before for cholesterol-rich eukaryotic rafts (Simons and Sampaio, 2011).

Additionally to providing more insight into FMM lipid composition of the model strain *B. subtilis* 168, we for the first time analysed the lipidome of the large-scale genome-minimized strain mini*Bacillus* PG10. Although Reuss *et al*. performed a detailed characterization of PG10 versus its Δ6 progenitor strain on the transcriptome, proteome and metabolome level (Reuß *et al*., 2017), their analysis did not include the lipidome. Our work indicates that the lipid composition of the membrane of PG10 and its initial progenitor strain, *B. subtilis* 168, is very similar. The most prominent change involved a decrease in the relative abundance of fatty acids in the membrane of PG10. This finding agrees with our RNA-seq analysis, in which a general trend of downregulation of fatty acid metabolic genes was observed in PG10. A possible cause for these observations is a reduced transcript level of *spo0A*, a major transcriptional regulator, which can activate and fine-tune the expression of the *accDA* operon during initiation of sporulation in *B. subtilis* (Pedrido *et al*., 2013; Haggett *et al*., 2018). Spo0A has been preserved during the genome reduction process and, in fact, displayed a ~ 2.5-fold decreased expression in PG10 (Table S2). This might have led to downregulation of the genes encoding the acetyl-CoA carboxylase complex (*accABCD*) and thus to a decreased production of malonyl-CoA (the substrate of fatty acid biosynthesis). As a consequence, fatty acid

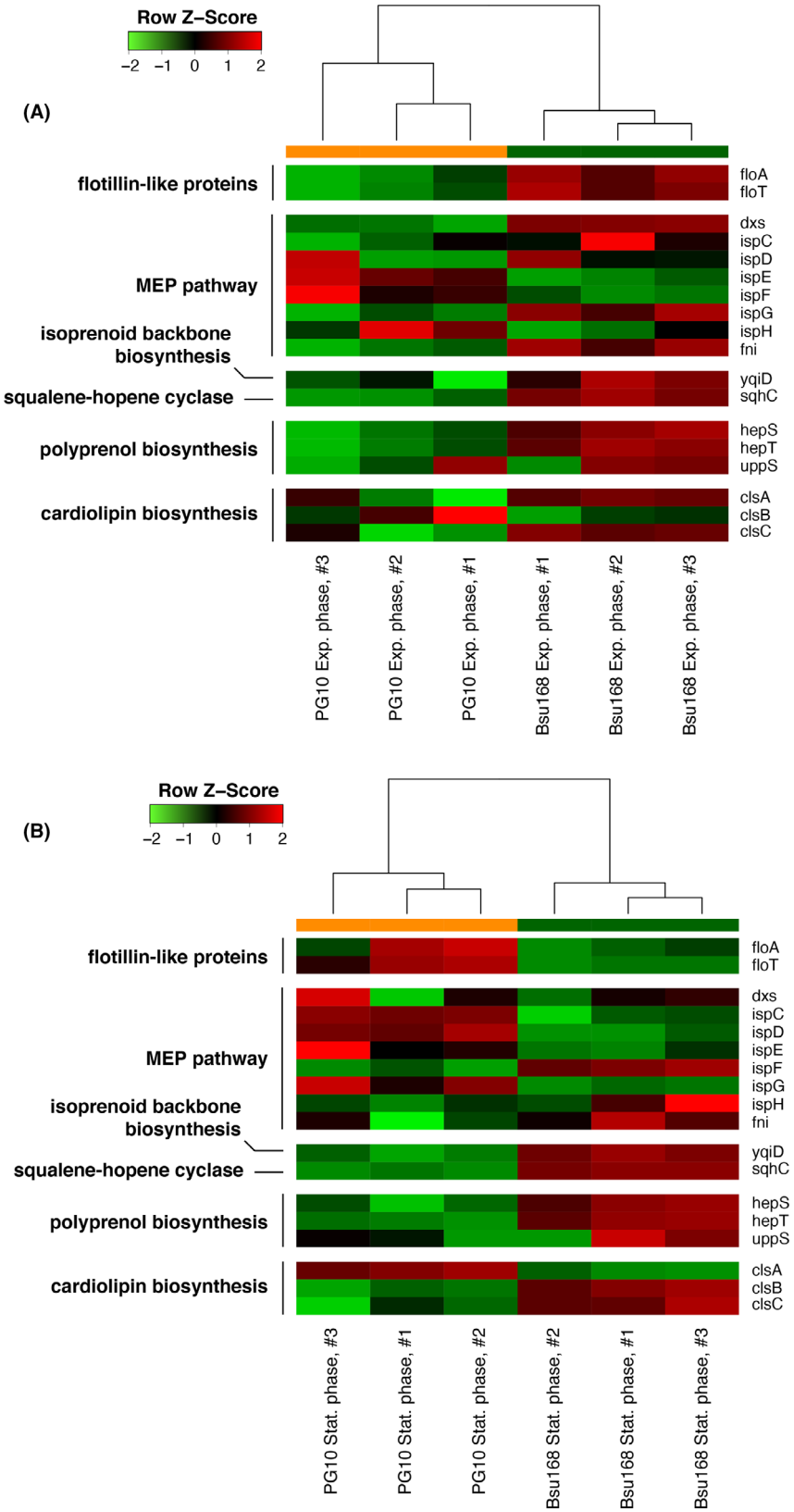

Fig. 8. Transcriptomic analysis of FMM lipid biosynthesis in *B. subtilis* 168 and PG10. Heatmaps of gene expression profiles of genes associated with FMM lipid biosynthesis of PG10 versus *B. subtilis* 168 in exponential (A) and stationary (B) phase.

Table 2. Differential expression levels of genes involved in FMM lipid biosynthesis between PG10 and *B. subtilis* 168. Only genes with fold change > 1.4 and FDR-adjusted *P*-value < 0.05 in the exponential (Exp.) and/ or stationary (Stat.) phase are shown.

Locus	Gene name	Function/pathway	Fold change PG10 vs. 168	
			Exp.	Stat.
BSU25380	*floA*	Flotillin-like protein	−2.6	
BSU31010	*floT*	Flotillin-like protein	−3.3	1.9
BSU24270	*dxs*	MEP pathway	−1.6	
BSU00900	*ispD*	MEP pathway		2.0
BSU00460	*ispE*	MEP pathway	1.7	
BSU00910	*ispF*	MEP pathway		−1.7
BSU25070	*ispG*	MEP pathway		1.9
BSU22870	*fni*	MEP pathway	−1.4	−2.1
BSU24280	*yqiD*	Geranyltransferase		−1.9
BSU19320	*sqhC*	Squalene–hopene cyclase	−1.7	−12.4
BSU22760	*hepS*	Polyprenol biosynthesis		−2.4
BSU22740	*hepT*	Polyprenol biosynthesis	−1.8	−5.6
BSU36590	*clsA*	Cardiolipin synthase, major enzyme		1.6
BSU37190	*clsB*	Cardiolipin synthase, minor enzyme	2.1	−3.4
BSU37240	*clsC*	Cardiolipin synthase, minor enzyme	−3.8	−2.5

biosynthetic genes became downregulated (possibly via FapR), resulting in a decreased level of fatty acids in PG10. At the same time, the cells possibly maintained the rate of incorporating fatty acids into phospholipids in order to maintain membrane homeostasis. Additionally, downregulation of genes involved in the degradation of fatty acids might have occurred to prevent further depletion of the fatty acid pool. In agreement with this, we indeed observed a reduced expression for the majority of genes involved in fatty acid biosynthesis and degradation, whereas phospholipid biosynthesis genes were less uniformly affected. Thus, although fatty acid metabolism seems to be deregulated in PG10, this did not come at the cost of membrane phospholipid homeostasis, since the phospholipid composition was similar between *B. subtilis* 168 and PG10.

By analysis of flotillin localization, membrane fluidity and DRM lipid composition, our work also gives a first indication of the existence and integrity of FMMs in PG10. Despite the large-scale genome reduction (including *yisP*), the lipidome profile of the DRM fraction in PG10 was found to be similar to the parental 168 strain, in terms of both DRM-enriched lipids and structural features of phospholipids in the different membrane fractions. The only difference observed was a significant increase in the relative abundance of CL, isoprenoids and hopanoids in the DRM fraction of PG10. Although this might suggest FMMs of PG10 to be even more compact than FMMs of *B. subtilis* 168, Laurdan staining experiments did not show drastic differences in overall or local membrane fluidity between the two strains. Additionally, distinct flotillin-enriched membrane domains could be observed in PG10. Thus, lack of *yisP* in PG10 did not seem to disturb the formation of FMMs. This is in contrast to what has been previously reported to occur in *B. subtilis* upon deletion of *yisP* (López and Kolter, 2010; Bach and Bramkamp, 2013). Perhaps, the large reduction in genome size led to changes in the regulatory landscape involved in maintenance of membrane heterogeneity in PG10. This might have enabled PG10 to cope with the absence of *yisP*, while preserving a heterogeneous membrane. In agreement with this, no large differences in the expression level of isoprenoid and CL biosynthesis genes were observed between PG10 and *B. subtilis* 168, in both exponentially and stationary growing cells. It thus seems that FMM integrity and the expression of the remaining FMM-relevant genes have been well maintained in PG10.

Strikingly, the reported and direct product of YisP, farnesol, could not be detected in any of the membrane fractions, neither in *B. subtilis* 168 nor in PG10 with reintroduced *yisP*. However, as a relatively hydrophilic isoprenoid lipid, farnesol might have ended up in the cytosolic fraction during the cell fractionation process. In addition, it is possible that farnesol is an intermediate in the biosynthesis of higher isoprenoid lipids and thus that it might have been converted into a variety of isoprenoid lipids of unknown nature. Interestingly, we did observe an increase in membrane fluidity in PG10 strains harbouring *yisP*. This finding agrees with previous studies reporting the ability of farnesol to fluidize and disorder biological membranes (Rowat and Davis, 2004; Inoue *et al*., 2016). Since farnesol was not detected in any of the membrane fractions analysed in this study, it remains unsure whether the increase in overall membrane fluidity in PG10 strains with *yisP* has been caused by farnesol itself. In addition, the increased membrane fluidity might also be (partly) attributed to the observed decrease in saturation level of phospholipid acyl chains in the non-raft membrane fraction of these strains. This latter finding suggests a secondary effect of reintroduction of *yisP* in PG10 and aligns with farnesol its behaviour to stabilize a fluid phase in membranes (Rowat and Davis, 2004).

Another interesting finding of our lipidomic analyses of the different strains is that there might be a certain level of codependency between the level of CL and isoprenoid lipids in FMMs. When comparing the lipid composition of DRM fractions between *B. subtilis* 168 and PG10, we observed a significant increase in both CL and isoprenoid lipids in the DRM fraction of PG10. In agreement with this, a decrease in CL as well as in isoprenoid lipids in the FMMs of PG10 was found upon deletion of the major CL synthase. These findings make it tempting to

speculate that CL and isoprenoid lipids are exclusive interaction partners within FMMs, and therefore influence each other's biosynthesis.

To conclude, our work clarifies which lipids reside in FMMs of *B. subtilis* and highlights structural features of raft and non-raft parts of the membrane. Moreover, we show that mini*Bacillus* PG10 still displays a heterogeneous membrane consisting of FMMs that are enriched in flotillins, CL and prenol lipids. This opens up the possibility to use FMMs both in *B. subtilis* 168 as well as in PG10 as spatial scaffolds for the potential improvement of heterologous multi-enzymatic production pathways.

Experimental procedures

Strains and growth conditions

Bacterial strains and plasmids used in this study can be found in Table 3. *Bacillus subtilis* 168 and mini*Bacillus* PG10 strains were cultured at 37°C with aeration in LB-Lennox medium (Formedium), unless otherwise stated. *E. coli* (Top10) was used as a cloning host and grown in LB at 37°C with aeration. When required, the growth media of *B. subtilis* strains were supplemented with antibiotics at the following concentrations: 0.5 μg ml^{-1} erythromycin, 12.5 μg ml^{-1} lincomycin or 5 μg ml^{-1} kanamycin. For PG10, half of the concentration of antibiotics was used in case of liquid cultures. For *E. coli*, 100 μg ml^{-1} ampicillin or 30 μg ml^{-1} kanamycin was used. For solid medium, growth media were supplemented with agar (1.5%).

Construction of plasmids and strains

Oligonucleotides used for cloning of plasmids can be found in Table S1 and were synthesized by Biolegio (Nijmegen, the Netherlands). Fast digest restriction enzymes, T4 DNA ligase and Phusion-HF DNA polymerase were purchased from Thermo Fisher Scientific (Waltham, MA, USA). PfuX7 DNA polymerase (purified in our laboratory) was used for colony PCR. Standard restriction–ligation was used for construction of plasmids. All constructs were verified by sequencing.

To integrate *floA* or *floT* fused to *GFP* controlled by their natural promoters (P_{yqeZ} and P_{yuaF}, respectively) in the *sacA* locus, two pJOE8999 vectors were generated. First, a specific single-guide RNA (sgRNA)-encoding sequence to target *sacA* was designed using the CRISPR Guide Design Software of Benchling (ggacgattttggatacatgt*)* and cloned into pJOE8999 via *BsaI* digestion. To allow homologous recombination, up- and downstream flanking regions of *sacA* were PCR amplified from genomic DNA of *B. subtilis* by using primer pairs sacA-up-fw-SfiI + sacA-up-rv-BglII (up) or sacA-down-fw-XhoI + sacA-down-rv-SfiI (down). To amplify

Table 3. List of plasmids and bacterial strains used in this study.

	Relevant characteristics	Reference
Plasmids		
pJOE8999	Vector for markerless genetic engineering of *B. subtilis* by employing CRISPR-Cas9; km^R	Altenbuchner (2016)
pJOE_FloA-GFP(sacA)	pJOE8999 derivative for insertion of *floA-GFP* under control of its native promoter (P_{yqeZ}) in the *sacA* locus	This study
pJOE_FloT-GFP(sacA)	pJOE8999 derivative for insertion of *floT-GFP* under control of its native promoter (P_{yuaF}) in the *sacA* locus	This study
pDG1664	Integration vector for genomic integration in the *thrC* locus of *B. subtilis* 168 and PG10; ery^R	Guérout-Fleury *et al*. (1996)
pDG-P_{nat}-yisP	pDG1664 derivative containing *yisP* controlled by its natural promoter	This study
pDG-P_{veg}-yisP	pDG1664 derivative containing *yisP* controlled by the strong constitutive promoter P_{veg}	This study
pUC21_ΔclsA	pUC21 derivative for deletion of *clsA*	Cao *et al*. (2017)
pSG-floA-GFP	pSG1154 carrying *floA-GFP*; source for amplification of *floA-GFP*	Gift of D. Lopez
pSG-floT-GFP	pSG1154 carrying *floT-GFP*; source for amplification of *floT-GFP*	Gift of D. Lopez
Strain		
B. subtilis 168	*trp*$^-$	Lab collection
B. subtilis 168 FloA-GFP	*B. subtilis* 168 derivative; *sacA::*P_{yqeZ}*-floA-GFP*	This study
B. subtilis 168 FloT-GFP	*B. subtilis* 168 derivative; *sacA::*P_{yuaF}*-floT-GFP*	This study
PG10	Large-scale genome-minimized strain derived from *B. subtilis* 168; 36% reduction in genome size	Reuß *et al*. (2017)
PG10 FloA-GFP	PG10 derivative; *sacA::*P_{yqeZ}*-floA-GFP*	This study
PG10 FloT-GFP	PG10 derivative; *sacA::*P_{yuaF}*-floT-GFP*	This study
PG10 Pnat-yisP	PG10 derivative; *thrC::*P_{nat}*-yisP*	This study
PG10 Pveg-yisP	PG10 derivative; *thrC::*P_{veg}*-yisP*	This study
PG10 Δ*clsA*	PG10 derivative; *clsA::kmR*	This study
E. coli Top10	*F– mcrA Δ(mrr-hsdRMS-mcrBC) Φ80lacZΔM15 ΔlacX74 recA1 araD139 Δ(ara leu) 7697 galU galK rpsL (StrR) endA1 nupG*	Lab collection

P_{yqeZ} and P_{yuaF} primer pairs PyqeZ-fw-BglII + PyqeZ-rv-ApaI or PyuaF-fw-BglII + PyuaF-rv-ApaI were used and using genomic DNA of *B. subtilis* as template DNA. *floA-GFP* and *floT-GFP* were amplified using forward primer floA-fw-ApaI or floT-fw-ApaI and reverse primer GFP-rv-XhoI, using as template DNA pSG-floA-GFP or pSG-floT-GFP. To obtain the final vectors, PCR fragments were digested with specified restriction enzymes and subsequently ligated into *SfiI*-digested pJOE vector containing the sgRNA-encoding sequence. This yielded the vectors pJOE_FloA-GFP(sacA) and pJOE_FloT-GFP (sacA).

To construct pDG1664 vectors containing *yisP* controlled by its natural promoter or by the strong constitutive P_{veg} promoter, the following primer pairs were used for amplification of different inserts from the genomic DNA of *B. subtilis:* Pnat-yisP-fw-Eco31I + yisP-rv-Eco31I (*yisP* and its promoter region), yisP-fw-Eco31I + yisP-rv-Eco31I (*yisP)* and Pveg-fw-Eco31I + Pveg-rv-Eco31I (P_{veg}). pDG1664 was linearized using primers pDG-bb-fw-Eco31I + pDG-bb-rv-Eco31I. Digestion of DNA fragments with Eco31I, followed by ligation, resulted in pDG-P_{nat}-yisP and pDG-P_{veg}-yisP.

B. subtilis 168 was transformed in Spizizen's minimal medium as described before (Harwood and Cutting, 1990). Competence in mini*Bacillus* PG10 was induced by supplementing LB medium with 0.5% (w/v) mannitol in the exponential phase (Rahmer *et al*., 2015).

Preparation of membrane fractions

Bacillus subtilis cell pellets, derived from stationary phase cultures, were re-suspended in lysis buffer (30 mM Tris-HCl pH 7.5 containing 1 mg ml^{-1} lysozyme and protease inhibitor cocktail) and incubated at 37°C for 30 min. Cells were lysed by sonication, and cell debris was removed by centrifugation (3000 *g*, 10 min, 4°C). The cell lysate was centrifuged at higher speed (175 000 *g*, 70 min, 4°C) to separate the cytosolic and membrane fraction. DSM and DRM fractions were prepared using the CelLytic MEM protein extraction kit (Sigma Aldrich, ST. Louis, MO, USA) according to manufacturer's instructions. In short, the membrane pellet was re-suspended in 800 µl of lysis and separation buffer by overnight incubation at 4°C with gentle agitation. The next morning, samples were centrifuged (3 min, 3000 *g*, RT) to remove material pelleting below the two phases. The two phases were mixed and incubated on ice for 10 min. Then, samples were incubated at 37°C for 30 min while inverting them a few times. By centrifugation (3 min, 3000 *g*, 25°C), the DSM fraction (upper phase) was subsequently separated from the DRM fraction (lower phase). Residual DSM was removed from the DRM fraction by a three times washing step involving resuspension of the DRM fraction in 400 µl of wash buffer, incubation for 10 min on ice and 20 min at 37°C. Centrifugation yielded again two phases of which the lower phase was used for subsequent washing steps and, in the end, to obtain the final DRM fraction. Three biological replicates of each membrane fraction of each strain were prepared for lipidomic analysis.

Protein detection by Western blotting

Detection of FloA or FloT (fused to GFP) was performed by loading samples (four times dilution of cytosolic fraction and three times dilution of DRM and DSM fractions) on a 10% SDS-PAGE gel. Blots were blocked for 1 h with 5% skimmed milk in PBST. For detection, primary antibodies were incubated O/N at 4°C, whereas secondary antibodies were incubated for 1 h at RT. The following antibodies were used: 1:5000 rabbit anti-GFP (G10362, Invitrogen) and 1:10 000 horseradish peroxidase-conjugated goat anti-rabbit (ABIN3020597, antibodies-online). Western blot signals were generated with Pierce ECL Plus Western blot substrate (GE Healthcare) and detected with the ChemiDoc XRS+ imaging system (Bio-Rad).

Fluorescence microscopy

For fluorescence microscopy, cells were immobilized on a microscope slide covered with a thin layer of 1.5% (w/v) agarose. Images were taken on a DeltaVision Elite inverted microscope (Applied Precision, GE Healthcare) equipped with a sCMOS camera, a four-colour fluorescent protein InsightSSI Module, and using a 100× oil, 1.4NA objective. For GFP images, an excitation wavelength 475/28 nm and emission wavelength 525/48 nm were used (1s exposure time, 32% power). Digital images were acquired with SoftWorX 3.6.0 software (Applied Precision) and analysed using ImageJ Fiji.

For Laurdan microscopy, a DAPI filter set was used for excitation at 390 nm and emission at 435 nm, whereas a FITC filter set was used for emission at 523 nm. Images were deconvolved, and ImageJ Fiji in combination with the macro tool CalculateGP (https://sils.fnwi.uva.nl/bcb/objectj/examples/CalculateGP/MD/gp.html, designed by Norbert Vischer) was used to calculate GP values and to generate heatmaps.

Laurdan labelling and spectroscopy

Laurdan (6-Dodecanoyl-N, N-dymethyl2-naphthylamine, Cayman Chemical Company) was used to assess membrane fluidity as previously described (Wenzel *et al*., 2018). Cells were grown in LB medium at 37°C and 220 rpm. At the desired OD_{600}, laurdan was added to a

final concentration of 10 μM from a 1 mM working solution dissolved in dimethylformamide (DMF). After 10 min incubation at 37°C in the dark, cells were washed three times in pre-warmed Laurdan Buffer and re-suspended to OD_{600} of 0.4.

For spectroscopic measurements, Laurdan was excited at 350 nm and fluorescent emission was measured at 460 and 500 nm using a plate reader (VarioskanLUX, Thermo Fisher). After subtraction of background fluorescence, GP values were calculated by using the following formula:

$$GP = I_{460} - I_{500}/I_{460} + I_{500}.$$

Lipid extraction

Lipid extraction from the membrane fractions was achieved by addition of isopropanol:methanol (1:1, v:v) (Honeywell, CHROMASOLV LC-MS Quality) containing internal standards (UltimateSPLASH ONE Cat. number 330820 Avanti lipids). The solution was sonicated for 30 min using the XX sonicator and spun down, and supernatant was subjected to analysis by LC-MS/MS.

Mass spectrometry

A Thermo Fisher Scientific Vanquish Autosampler – HPLC-platform was used with a 100 mm BEH C18 column with inner diameter 2.1 mm and particle size 1.7 μm (Waters, Milford, MA, USA). All solvents were prepared with H_2O from an Ultrapure IQ7000 system with a LC-Pak Polisher (Merck Millipore, Burlington, MA, USA). Solvent A acetonitrile:H_2O (60:40, v:v) containing 10 mM ammonium acetate. Solvent B, isopropanol:acetonitrile (90:10, v:v) containing 10 mM ammonium acetate. Chromatographic separation was achieved by starting with 85% solvent A and 15% solvent B; percentage of solvent B is given at decimal time in min: [(0 : 15%), (3.88 : 30%), (4.95 : 48%), (21.96 : 82%), (23.03 : 99%), (24.24 : 15%), (30 : 15%), end]. Valve position, 0–8.3 min into waste, 8.3–23.03 min mass spectrometer, 23.03–30 min into waste. Flow rate was 0.4 ml min^{-1} with a single injection volume of 3 μl per sample. A Thermo Fisher Scientific Q-Exactive Orbitrap mass spectrometer with a heated electrospray ionization source was operated in polarity switching ionization mode (capillary temp. 300°C) at 60 000 resolution with an acquisition cycle of MS1 and Top20 MS2.

Spectral data processing and data analysis

The software COMPOUND DISCOVERER 3.1 of Thermo Fisher Scientific was used to align, group, integrate and annotate the peaks from mass spectrometry raw data using an in-house lipid database based on MS1. Statistical analysis was performed using python 3.6 with the latest (10.7.2020) libraries of the SciPy ecosystem and seaborn.

RNA isolation and quality control

For RNA-seq analysis, cells were grown in LB medium at 37°C and 220 rpm and harvested in the mid- to late-exponential phase or stationary phase. Cell pellets were re-suspended in 200 μl of TE buffer, after which 1% (final) SDS and 0.25 g of glass beads were added. After two times bead beating for 1 min (1 min on ice in between), 1 ml of ice-cold TRIzol was added and samples were vortexed and incubated for 20 min at 70°C to fully lyse the cells. 200 μl of chloroform was then added, followed by vortexing for 15 s and incubation for 2 min at RT. After centrifugation (12 500 *g*, 15 min, 4°C), the upper aqueous phase containing RNA was transferred to a clean tube and mixed with two volumes of 100% ethanol. RNA was purified using an RNA Clean & Concentrator™-5 column (Zymo Research, cat. R1015) according to manufacturer instructions. RNA concentrations were measured using a NanoDrop ND-1000 (Thermo Fisher Scientific). RNA quality was assessed by gel electrophoresis. RNA samples were stored at −80°C.

RNA sequencing and data analysis

rRNA depletion and cDNA library preparation were performed using Zymo-Seq RiboFree Total RNA-Seq Library Kit (Zymo Research, cat. 3003). Fastq files were mapped to the *B. subtilis* str. 168 reference genome (accession: NC_000964.3) using Bowtie (Langmead *et al*., 2009) (parameters: -a -l 28 -n 2 -m 7 --best --strata). Counts per gene were calculated using featureCounts (Liao *et al*., 2014) and the latest RefSeq annotation (parameters: -t gene -g locus_tag -O -M --fraction). Differentially expressed genes were identified using DESeq2 (Love *et al*., 2014), selecting genes with an absolute log2(fold change) $\geq$ 0.5 and FDR-adjusted *P*-value < 0.05.

Acknowledgements

We thank Julius Fülleborn for his help with reintroduction of YisP in PG10. We thank Anne de Jong for his help with RNA-seq sample preparation. We thank Alaa Othman for his support on lipid analysis. We thank Daniel López for kindly providing pSG1154 plasmids containing *floA-GFP* or *floT-GFP*. A.Y.v.T., P.W. and A.J.v.H. were supported by a grant from the European Union's Horizon 2020 research and innovation program (Grant Agreement No. 720776).

Conflict of interest

The authors declare no competing financial interest.

Author contributions

AYT, OPK and US conceived the study. AYT and PW designed, performed and analysed experiments, wrote the manuscript and prepared figures. AJH contributed to the design of the experiments, data analysis and interpretation of the results. All authors contributed to correction of the manuscript.

Data availability statement

RNA-seq data from this study have been submitted to the NCBI Gene Expression Omnibus under accession number GSE169409. Lipidomics data have been submitted at the MetaboLights database under accession number MTBLS2711, and the extracted lipidomics data are available in tabular format (Data S1).

References

Aguilar Suárez, R., Stülke, J., and Van Dijl, J.M. (2019) Less is more: toward a genome-reduced *Bacillus* cell factory for "difficult proteins". *ACS Synth Biol* **8:** 99–108.

Altenbuchner, J. (2016) Editing of the *Bacillus subtilis* genome by the CRISPR-Cas9 system. *Appl Environ Microbiol* **82:** 5421–5427.

Bach, J.N., and Bramkamp, M. (2013) Flotillins functionally organize the bacterial membrane. *Mol Microbiol* **88:** 1205–1217.

Belin, B.J., Busset, N., Giraud, E., Molinaro, A., Silipo, A., and Newman, D.K. (2018) Hopanoid lipids: from membranes to plant – bacteria interactions. *Nat Rev Microbiol* **16:** 304–315.

Bernat, P., Paraszkiewicz, K., Siewiera, P., Moryl, M., Plaza, G., and Chojniak, J. (2016) Lipid composition in a strain of *Bacillus subtilis*, a producer of iturin A lipopeptides that are active against uropathogenic bacteria. *World J Microbiol Biotechnol* **32:** 157.

Bramkamp, M., and Lopez, D. (2015) Exploring the existence of lipid rafts in bacteria. *Microbiol Mol Biol Rev* **79:** 81–100.

Brown, D.A. (2002) Isolation and use of rafts. *Curr Protoc Immunol* **51.** Chapter 11:Unit 11.10. https://doi.org/10.1002/0471142735.im1110s51

Cao, H., Heel, A.J., Ahmed, H., Mols, M., and Kuipers, O.P. (2017) Cell surface engineering of *Bacillus subtilis* improves production yields of heterologously expressed α-amylases. *Microb Cell Fact* **16:** 56.

Carquin, M., D'Auria, L., Pollet, H., Bongarzone, E.R., and Tyteca, D. (2016) Recent progress on lipid lateral heterogeneity in plasma membranes: from rafts to submicrometric domains. *Prog Lipid Res* **62:** 1–24.

Chwastek, G., Surma, M.A., Rizk, S., Grosser, D., Lavrynenko, O., Rucińska, M., *et al*. (2020) Resource principles of membrane adaptation revealed through environmentally induced bacterial lipidome remodeling. *Cell Rep* **32:** 108165.

Donovan, C., and Bramkamp, M. (2009) Characterization and subcellular localization of a bacterial flotillin homologue. *Microbiology* **155:** 1786–1799.

Doughty, D.M., Dieterle, M., Sessions, A.L., Fischer, W.W., and Newman, D.K. (2014) Probing the subcellular localization of hopanoid lipids in bacteria using NanoSIMS. *PLoS One* **9:** e84455.

Fahy, E., Subramaniam, S., Brown, H.A., Glass, C.K., Merrill, A.H., Murphy, R.C., *et al*. (2005) A comprehensive classification system for lipids. *J Lipid Res* **46:** 839–861.

Fahy, E., Subramaniam, S., Murphy, R.C., Nishijima, M., Raetz, C.R.H., Shimizu, T., *et al*. (2009) Update of the LIPID MAPS comprehensive classification system for lipids. *J Lipid Res* **50:** 9–14.

Feng, X., Hu, Y., Zheng, Y., Zhu, W., Li, K., Huang, C.H., *et al*. (2014) Structural and functional analysis of *Bacillus subtilis yisP* reveals a role of its product in biofilm production. *Chem Biol* **21:** 1557–1563.

García-Fernández, E., Koch, G., Wagner, R.M., Fekete, A., Stengel, S.T., Schneider, J., *et al*. (2017) Membrane microdomain disassembly inhibits MRSA antibiotic resistance. *Cell* **171:** 1354–1367.

Gidden, J., Denson, J., Liyanage, R., Ivey, D.M., and Lay, J.O. (2009) Lipid compositions in *Escherichia coli* and *Bacillus subtilis* during growth as determined by MALDI-TOF and TOF/TOF mass spectrometry. *Int J Mass Spectrom* **283:** 178–184.

Guérout-Fleury, A.-M., Frandsen, N., and Stragier, P. (1996) Plasmids for ectopic integration in *Bacillus subtilis*. *Gene* **180:** 57–61.

Haggett, L., Bhasin, A., Srivastava, P., and Fujita, M. (2018) A revised model for the control of fatty acid synthesis by master regulator Spo0A in *Bacillus subtilis*. *Mol Microbiol* **108:** 424–442.

Harwood, C.R., and Cutting, S.M. (1990) *Molecular Biological Methods for Bacillus*. Chichester, UK: John Wiley and Sons.

Inoue, Y., Togashi, N., and Hamashima, H. (2016) Farnesol-induced disruption of the *Staphylococcus aureus* cytoplasmic membrane. *Biol Pharm Bull* **39:** 653–656.

Kawai, F., Shoda, M., Harashima, R., Sadaie, Y., Hara, H., and Matsumoto, K. (2004) Cardiolipin domains in *Bacillus subtilis* Marburg membranes. *J Bacteriol* **186:** 1475–1483.

Langmead, B., Trapnell, C., Pop, M., and Salzberg, S.L. (2009) Ultrafast and memory-efficient alignment of short DNA sequences to the human genome. *Genome Biol* **10:** R25.

Liao, Y., Smyth, G.K., and Shi, W. (2014) featureCounts: an efficient general purpose program for assigning sequence reads to genomic features. *Bioinformatics* **30:** 923–930.

Lopez, D., and Koch, G. (2017) Exploring functional membrane microdomains in bacteria: an overview. *Curr Opin Microbiol* **36:** 76–84.

López, D., and Kolter, R. (2010) Functional microdomains in bacterial membranes. *Genes Dev* **24:** 1893–1902.

Love, M.I., Huber, W., and Anders, S. (2014) Moderated estimation of fold change and dispersion for RNA-seq data with DESeq2. *Genome Biol* **15:** 550.

Lv, X., Wu, Y., Tian, R., Gu, Y., Liu, Y., Li, J., *et al*. (2020) Synthetic metabolic channel by functional membrane microdomains for compartmentalized flux control. *Metab Eng* **59:** 106–118.

Michalik, S., Reder, A., Richts, B., Faßhauer, P., Mäder, U., Pedreira, T., *et al*. (2021) The *Bacillus subtilis* minimal genome compendium. *ACS Synth Biol* **10:** 2767–2771.

Otto, G.P., and Nichols, B.J. (2011) The roles of flotillin microdomains-endocytosis and beyond. *J Cell Sci* **124:** 3933–3940.

Pedrido, M.E., de Oña, P., Ramirez, W., Leñini, C., Goñi, A., and Grau, R. (2013) Spo0A links de novo fatty acid synthesis to sporulation and biofilm development in *Bacillus subtilis*. *Mol Microbiol* **87:** 348–367.

Poger, D., and Mark, A.E. (2013) The relative effect of sterols and hopanoids on lipid bilayers: when comparable is not identical. *J Biol Chem* **117:** 16129–16140.

Rahmer, R., Heravi, K.M., and Altenbuchner, J. (2015) Construction of a super-competent *Bacillus subtilis* 168 using the *PmtlA-comKS* inducible cassette. *Front Microbiol* **6:** 1431.

Reuß, D.R., Altenbuchner, J., Mäder, U., Rath, H., Ischebeck, T., Sappa, P.K., *et al*. (2017) Large-scale reduction of the *Bacillus subtilis* genome: consequences for the transcriptional network, resource allocation, and metabolism. *Genome Res* **27:** 289–299.

Rowat, A.C., and Davis, J.H. (2004) Farnesol-DMPC phase behaviour: a 2H-NMR study. *Biochim Biophys Acta* **1661:** 178–187.

Sáenz, J.P., Grosser, D., Bradley, A.S., Lagny, T.J., Lavrynenko, O., Broda, M., and Simons, K. (2015) Hopanoids as functional analogues of cholesterol in bacterial membranes. *Proc Natl Acad Sci USA* **112:** 11971–11976.

Saenz, J.P., Sezgin, E., Schwille, P., and Simons, K. (2012) Functional convergence of hopanoids and sterols in membrane ordering. *Proc Natl Acad Sci USA* **109:** 14236–14240.

Schneider, J., Klein, T., Mielich-Süss, B., Koch, G., Franke, C., Kuipers, O.P., *et al*. (2015) Spatio-temporal remodeling of functional membrane microdomains organizes the signaling networks of a bacterium. *PLOS Genet* **11:** e1005140.

Sezgin, E., Levental, I., Mayor, S., and Eggeling, C. (2017) The mystery of membrane organization: composition, regulation and roles of lipid rafts. *Nat Rev Mol Cell Biol* **18:** 361–374.

Simons, K., and Ikonen, E. (1997) Functional rafts in cell membranes. *Nature* **387:** 569–572.

Simons, K., and Sampaio, J.L. (2011) Membrane organization and lipid rafts. *Cold Spring Harb Perspect Biol* **3:** 1–17.

van Tilburg, A.Y., Fülleborn, J.A., Reder, A., Völker, U., Stülke, J., van Heel, A.J., and Kuipers, O.P. (2021) Unchaining mini*Bacillus* strain PG10: relief of FlgM-mediated repression of autolysin genes. *Appl Environ Microbiol* **87:** e01123-21.

van Tilburg, A.Y., van Heel, A.J., Stülke, J., de Kok, N.A.W., Rueff, A.S., and Kuipers, O.P. (2020) Mini*Bacillus* PG10 as a convenient and effective production host for lantibiotics. *ACS Synth Biol* **9:** 1833–1842.

Wenzel, M., Vischer, N., Strahl, H., and Hamoen, L. (2018) Assessing membrane fluidity and visualizing fluid membrane domains in bacteria using fluorescent membrane dyes. *Bio-Protocol* **8:** e3063.

Zielińska, A., Savietto, A., de Sousa Borges, A., Martinez, D., Berbon, M., Roelofsen, J.R., *et al*. (2020) Flotillin mediated membrane fluidity controls peptidoglycan synthesis and MreB movement. *eLife* **9:** e57179.

Supporting information

Additional supporting information may be found online in the Supporting Information section at the end of the article.

Fig. S1. Lipidome profiles of total membrane fractions of *B. subtilis* 168 and PG10. (A) TIC normalized relative abundance of lipid classes in total membrane fractions of *B. subtilis* 168 and PG10. (B) Log2 fold change of relative abundance of lipid classes in total membrane fractions of PG10 versus *B. subtilis* 168. Abbreviations: cardiolipin (CL), polyprenol (Po), phosphatidylethanolamine (PE), diacylglycerol (DAG), isoprenoids (Is), lysophosphatidic acid (LPA), fatty acids (FA), phosphatidylglycerol (PG), quinones (Qu), phosphatidylserine (PS), monoacylglycerol (MAG), lysophosphatidylglycerol (LPG), lysophosphatidylethanolamine (LPE), lysophosphatidylserine (LPS) and hopanoids (Ho).

Fig. S2. Structural attributes of annotated prenol lipids. Representation of the structural attributes of detected prenol lipids. The most abundant lipid of each class is highlighted with an asterisk. Abbreviations: hopanoids (Ho), isoprenoids (Is), polyprenol (Po) and quinones (Qu).

Fig. S3. Chromatograms and ms2 information of cardiolipins and isoprenoids in different strains. Abundant cardiolipin (CL) and isoprenoid (Is) species with corresponding MS2 information. 'dclsA' is the PG10 *clsA* deletion strain.

Fig. S4. Structural comparison of glycerophospholipids in *B. subtilis* 168 and PG10 across different membrane fractions. Cluster map of z-scored relative lipid abundances of the main phospholipids in B. subtilis 168 and PG10 between the total membrane (TM), detergent-sensitive membrane fraction (DSM) and detergent-resistant membrane fraction (DRM). Abbreviations: cardiolipin (CL), phosphatidylglycerol (PG) and phosphatidylethanolamine (PE).

Fig. S5. FMM composition of mini*Bacillus* PG10 strains with different genetic backgrounds. Abundancies of lipid classes in DRM fractions of different PG10 strains: deletion of *clsA* ('dclsA'), reintroduction of *yisP* controlled by its natural promoter ('nat') or the P_{veg} constitutive promoter ('veg').

Fig. S6. Analysis of gene expression profiles' similarity of *B. subtilis* 168 and PG10 in exponential and stationary growth phase. (A) PCA analysis. Exp. = exponential phase and Stat. = stationary phase. Replicates are labelled #1-3. (B) Correlation analysis of gene expression profiles of the same conditions as mentioned in (A).

Table S1. List of oligonucleotides used in this study.

Table S2. Differential expression level of *spo0A* in PG10 compared with *B. subtilis* 168.

Data S1. Extracted lipidomics data.

